Quantum Coherent Energy Transfer over Varying Pathways in Single Light-Harvesting Complexes

Richard Hildner *et al.*

Science **340**, 1448 (2013);
DOI: 10.1126/science.1235820

Science (print ISSN 0036-8075; online ISSN 1095-9203) is published weekly, except the last week in December, by the American Association for the Advancement of Science, 1200 New York Avenue NW, Washington, DC 20005.

Quantum Coherent Energy Transfer over Varying Pathways in Single Light-Harvesting Complexes

Richard Hildner,[1]* Daan Brinks,[1]† Jana B. Nieder,[1] Richard J. Cogdell,[2] Niek F. van Hulst[1,3]‡

The initial steps of photosynthesis comprise the absorption of sunlight by pigment-protein antenna complexes followed by rapid and highly efficient funneling of excitation energy to a reaction center. In these transport processes, signatures of unexpectedly long-lived coherences have emerged in two-dimensional ensemble spectra of various light-harvesting complexes. Here, we demonstrate ultrafast quantum coherent energy transfer within individual antenna complexes of a purple bacterium under physiological conditions. We find that quantum coherences between electronically coupled energy eigenstates persist at least 400 femtoseconds and that distinct energy-transfer pathways that change with time can be identified in each complex. Our data suggest that long-lived quantum coherence renders energy transfer in photosynthetic systems robust in the presence of disorder, which is a prerequisite for efficient light harvesting.

Highly efficient excitation energy transfer is a key step in the initial light-driven processes of photosynthesis and takes place in sophisticated supramolecular assemblies, so-called pigment-protein complexes (*1*, *2*). Much work has been devoted to revealing the underlying mechanisms and to understanding the spatial and energetic organization of the pigment molecules involved (*1*–*8*). A particularly intriguing question that recently emerged concerns the impact of quantum coherence on promoting the efficiency and the directionality of ultrafast energy transport in photosynthesis. Although the presence of this quantum effect is now generally accepted (*9*), many open questions associated with this phenomenon remain, including how light-harvesting antennae evolved to be robust against perturbations and thermal disorder under physiological conditions and whether quantum coherent transport can help to optimize the energy flow despite the presence of disorder. Owing to the large structural and electronic heterogeneity of photosynthetic antenna proteins (*10*–*12*), such issues are not testable by conventional femtosecond spectroscopy (*2*–*5*).

We addressed these questions by using an ultrafast single-molecule technique (*13*, *14*) to study a prototypical antenna protein, the light-harvesting 2 (LH2) complex from the purple bacterium *Rhodopseudomonas acidophila*. In this assembly, 27 bacteriochlorophyll a (Bchl a) molecules are arranged in two concentric rings (Fig. 1A) that give rise to the characteristic near-infrared absorption bands (Fig. 1B), labeled according to their absorption maxima, B800 (with 9 weakly coupled Bchl a pigments) and B850 (with 18 strongly coupled Bchl a). Because the B800-B850 transfer within these complexes is governed by an intermediate electronic coupling (*7*, *8*), we are particularly interested in the role of quantum coherence in the transport between these energy eigenstates.

The femtosecond coherent B800-B850 dynamics in single LH2 complexes were studied by a specific two-color experiment. A Fourier-limited 15-fs pulse was phase-shaped into two time-delayed transform limited pulses with different carrier frequencies that overlap with the B800 and B850 absorptions of LH2, respectively (Fig. 1C). This was achieved by selectively applying a linear phase ramp to the appropriate spectral band in a pulse shaper (Fig. 1B, green line), which gives full control over the delay time, Δt, as well as the relative carrier envelope phase, $\Delta\phi$, between both pulses. We detected the fluorescence signal, that is, the total population probability of the lowest-

[1]ICFO–Institut de Ciencies Fotoniques, Mediterranean Technology Park, 08860 Castelldefels (Barcelona), Spain. [2]Institute of Molecular, Cell, and Systems Biology, College of Medical, Veterinary, and Life Sciences, University of Glasgow, Glasgow G12 8TA, UK. [3]ICREA–Institució Catalana de Recerca i Estudis Avançats, 08015 Barcelona, Spain.

*Present address: Experimentalphysik IV, Universität Bayreuth, 95440 Bayreuth, Germany.

†Present address: Department of Chemistry and Chemical Biology, Harvard University, Cambridge, MA 02138, USA.

‡Corresponding author. E-mail: niek.vanhulst@icfo.eu

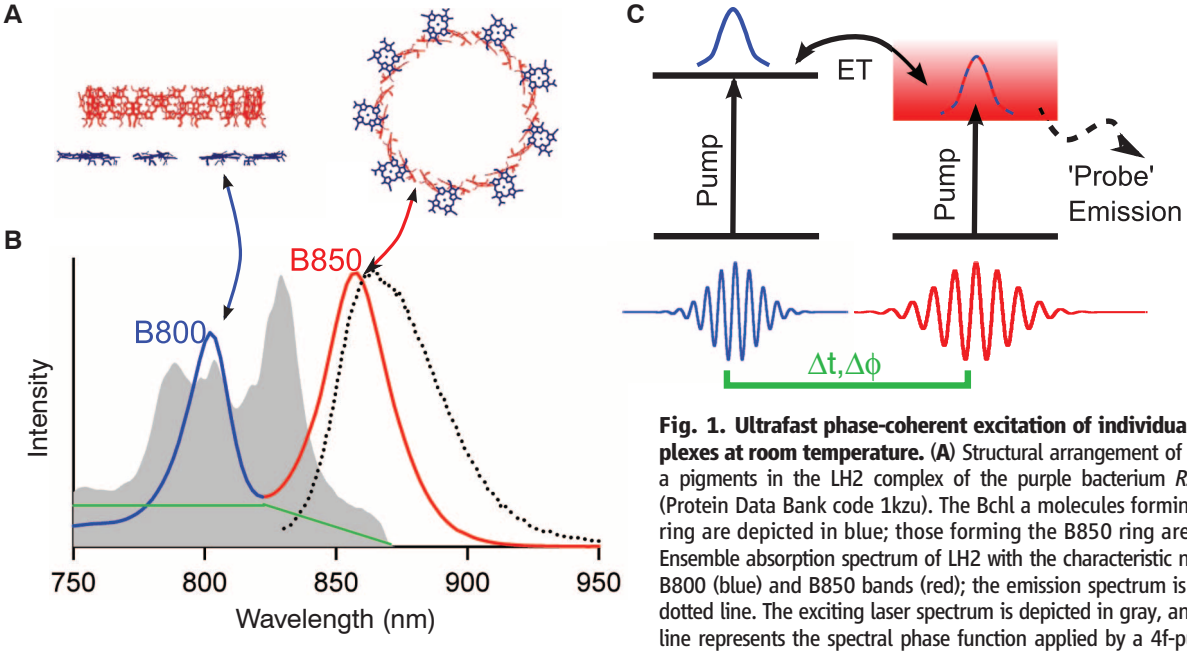

Fig. 1. Ultrafast phase-coherent excitation of individual LH2 complexes at room temperature. (**A**) Structural arrangement of the 27 Bchl a pigments in the LH2 complex of the purple bacterium *R. acidophila* (Protein Data Bank code 1kzu). The Bchl a molecules forming the B800 ring are depicted in blue; those forming the B850 ring are in red. (**B**) Ensemble absorption spectrum of LH2 with the characteristic near-infrared B800 (blue) and B850 bands (red); the emission spectrum is shown as a dotted line. The exciting laser spectrum is depicted in gray, and the green line represents the spectral phase function applied by a 4f-pulse shaper. (**C**) Concept of the experiment: Single LH2 are excited by a two-color pulse pair with Δt and $\Delta\phi$ generated by applying the spectral phase function. The first pulse (blue) creates an excitation in the B800 band. After energy transfer (ET) to the B850 band, the second time-delayed pulse (red), resonant with the B850 band, modulates the population transfer to the B850 excited states by quantum interference and thus changes the probe signal, the spontaneous emission from a single complex.

energy and emitting B850 exciton state after interaction with both pulses. The spectral amplitudes were the same for all (Δt, $\Delta\phi$) combinations in our experiments (for details, see materials and methods in the supplementary materials).

In a first experiment, we varied the delay time Δt while keeping the relative carrier phase $\Delta\phi$ constant. Individual LH2 complexes feature pronounced oscillations in their emission as a function of Δt up to at least 400 fs, as shown for two representative examples (Fig. 2, B and C). Although both complexes exhibit oscillation periods of around 200 fs and contrasts of about 15% (ratio between maximum and minimum signal), there are differences in their ultrafast B800-B850 transfer dynamics. In order to quantify this femtosecond response, we retrieved the oscillation periods, T, from the delay traces by a cosine fit to the data. The resulting histogram (Fig. 2D) features a wide distribution between 140 and 400 fs with a maximum near 200 fs. This broad spread in T demonstrates the large structural and electronic disorder between complexes that is caused by the heterogeneous local dielectric protein environment (*15*, *16*). This disorder is typically hidden in ensemble experiments but has a substantial impact on the specific B800-B850 transport within each complex. Because the dynamics of this transfer depend on the site energies as well as on the mutual orientations and distances of the involved pigments, that is, on their particular electronic couplings, these different ultrafast responses imply that each complex features a distinct transfer pathway characterized by its period T (see fig. S3 and accompanying text for more details on resolving this heterogeneity and different pathways). On the basis of an analytical treatment, the distribution of T is consistent with an average electronic coupling of $J \approx 50\ \mathrm{cm}^{-1}$ between B800 and high-energy B850 states (see supplementary materials), which is in agreement with ensemble experiments and theory (*3*, *5*) and indicates that optically dark high-energy B850 exciton states are involved in these first transfer steps.

We attribute the oscillations in Fig. 2, B and C, to quantum interference between two excitation pathways that populate the same target state, the emitting lowest-energy B850 level. Single complexes are first excited with a broadband short-wavelength pulse ($\Delta t > 0$) that is resonant with B800 and thus creates an excitation in this band. This excitation evolves under field-free conditions during the time interval Δt. In particular, electronic coupling mixes B800 and B850 states, and the total wave function can be expressed as $|\Psi\rangle = c_{B800}|\psi_{B800}\rangle + c_{B850}|\psi_{B850}\rangle$; that is, an electronic coherence between B800 and B850 is induced by the electronic B800-B850 coupling. After relaxation to optically allowed low-energy B850 excited states, the delayed longer wavelength pulse then either enhances or reduces the population of the emitting B850 level by quantum interference. This effect depends critically on the survival time of quantum coherence in the system (see fig. S2 and accompanying text), for which several mechanisms have been proposed (*16*–*19*). In contrast, if the electronic coherence decayed rapidly within ~50 fs, as usually expected for a disordered system at room temperature, we would observe a constant emission as a function of Δt, except for a short interval $\Delta t \leq 50$ fs where phase memory is present (*14*).

The electronic nature of the coherences giving rise to the oscillatory delay traces (Fig. 2, B and C) was confirmed by control experiments on LH2 (fig. S6) and by recent two-dimensional spectroscopy on isolated (*20*) and protein-bound Bchl a pigments (*21*–*24*). Consequently, the persistent oscillations in the traces in Fig. 2, B and C, are a signature that electronic quantum coherences between B800 and B850 survive for an unexpectedly long time, at least 400 fs, in individual LH2 complexes under physiological conditions. Similar quantum effects have been reported by Lee *et al*. and Harel *et al*., who observed coherences between electronic eigenstates in light-harvesting antenna proteins by ensemble photon-echo methods (*21*, *25*).

A crucial question concerns the role of coherence in the robustness of energy transport against external perturbations, such as conformational fluctuations, that occur in LH2 on time scales of seconds (*10*) and modify the electronic couplings between pigments on such slow time scales. To investigate this issue, we resolved phase changes in the energy transfer by recording the fluorescence of individual complexes as a function of the relative carrier envelope phase $\Delta\phi$ at constant Δt. The delay time was chosen to be longer than 100 fs to avoid pulse-overlap effects but well below 400 fs to remain in the coherent regime. This phase-cycling measurement (Fig. 3, red symbols) features a full sinusoidal period of the emission upon a relative phase change of more than 2π at $\Delta t = 150$ fs. A comparison with the reference signal from the same complex (Fig. 3, open black circles), taken repeatedly with a Fourier-limited pulse encompassing the full laser spectrum, shows that the excitation probability is enhanced by 15% for a relative phase of about 0.5π (and reduced by 15% for a relative phase of $\sim 1.5\pi$). This observation demonstrates weak-field phase control of the quantum interference between the excitation pathways to B800 and B850 excited states or, in other words, phase control of the efficiency of the coherent contribution to the functionally important B800-B850 transfer pathway.

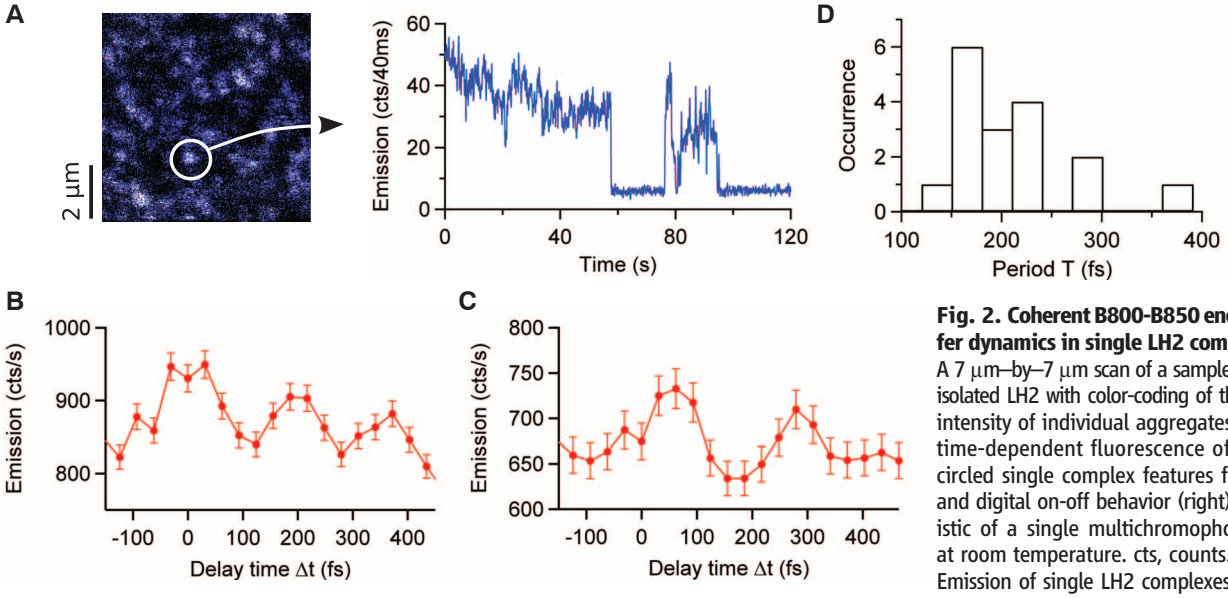

Fig. 2. Coherent B800-B850 energy transfer dynamics in single LH2 complexes. (A) A 7 µm–by–7 µm scan of a sample containing isolated LH2 with color-coding of the emission intensity of individual aggregates (left). The time-dependent fluorescence of the white circled single complex features fluctuations and digital on-off behavior (right) characteristic of a single multichromophoric system at room temperature. cts, counts. (**B** and **C**) Emission of single LH2 complexes as a function of the interpulse delay time with constant relative carrier envelope phase, demonstrating coherent population oscillations between B800 and B850 bands with very long coherence times of hundreds of femtoseconds. Error bars indicate ±1 SD based on a total number of $N = 4 \times 10^3$ (B) and 1.5×10^3 (C) photons. (**D**) Histogram of the oscillation period T retrieved from traces as shown in (B) and (C).

Such efficient phase control indicates that the time scale for B800-B850 population transfer (*1*, *2*) is comparable to that for dissipative interactions with the local (protein) bath (*26*, *27*).

Notable variations in the ultrafast response of single complexes were tracked with our rapid phase-cycling approach (Fig. 4 and fig. S5). As an example, Fig. 4A presents the raw data from an individual aggregate. Each block with about 8-s measurement time represents a phase scan from 0 to 2π at a constant interpulse delay of 100 fs. Whereas the (temporal) average over the entire 120-s measurement (Fig. 4B, green symbols) is basically identical to the reference signal (open black symbols) and does not reveal phase-sensitive features, analyzing shorter time intervals of the data gives a completely different picture (Fig. 4C): The red circles depict the emission as a function of phase for the first ~35 s of observation time, and the blue circles show the fluorescence at later times. The observed jump of the oscillation phase by about π demonstrates a change in the ultrafast response of this single complex after some 10 s. This phase jump must result from a change of the accumulated phase of the relaxing excitation (supplementary materials), because the experimental conditions were the same throughout the entire measurement. This jump implies a modification of the energy transfer pathway from B800 toward possibly different low-energy, optically accessible B850 excited states (e.g., the ±1 exciton levels) caused by subtle structural rearrangements in the complex (*10*, *11*) that alter mutual distances and angles between the Bchl a pigments as well as their site energies because of different local interactions. The amplitude of the phase-dependent modulation remains basically constant, although the phase relation is inverted, which indicates persistent coherence even for changing transfer pathways.

Both ensemble and temporal averaging washes out all features observed in the subsets of the data, as illustrated in the total average in Fig. 4B and fig. S5 (open green symbols). Hence, experiments integrating over too long time scales or on ensembles of many complexes would lead to the unjustified conclusion that phase memory was already completely lost within Δt = 100 fs. These data demonstrate that only single-molecule detection allows all subtle details of a complex system in the presence of thermal disorder to be revealed.

Persistent quantum coherences in photosynthetic complexes were previously attributed to correlated nuclear motions of the pigments' local dielectric environments that give rise to long-lived site energy cross-correlations (*21*, *22*, *25*, *28*), whereas subsequent molecular dynamics simulations have failed to reproduce such correlated protein fluctuations (*16*, *18*). However, this latter work indicates that coherences in antenna complexes can still survive hundreds of fs as long as the electronic coupling between pigments is strong enough and does not change on the relevant time scales (*16*). Moreover, it has very recently been suggested that interactions with discrete bath modes featuring energies similar to energy differences of exciton states may help to sustain long-lived coherent energy transport (*17*). For the biological function of LH2, it is the interplay between this persistent coherence and energy dissipation by interactions with the surrounding bath (*19*, *29*–*31*) that rapidly directs the excitation energy toward the lowest-energy B850 target levels, from which further transfer to adjacent LH2 or LH1 occurs. Dissipative interactions, on one hand, stabilize the initially created electronic excitations in lower-energy states on sub-ps time scales to create the ultrafast energy funnel to bottom B850 states and to prevent relaxation along loss channels. On the other hand, quantum coherences survive long enough to allow averaging over local inhomogeneities of the rough excited-state energy landscape and thus to avoid trapping in local minima. The highest efficiencies for this environmentally assisted quantum transfer in photosynthetic light-harvesting complexes have been found for comparable time scales of population transfer and dissipative relaxation (*29*–*31*). This requirement is fulfilled for the B800-B850 transfer, as shown in Figs. 3 and 4, by efficient weak-field phase control of the one-photon transitions into the B800 and B850 excited states.

An intriguing feature of our observations is that the quantum beats are rather well-defined compared with ensemble data and can be described by only a single oscillatory component. Hence, it seems that in each specific LH2 complex only one energy transfer pathway at a time is present. Because a rather large number of pig-

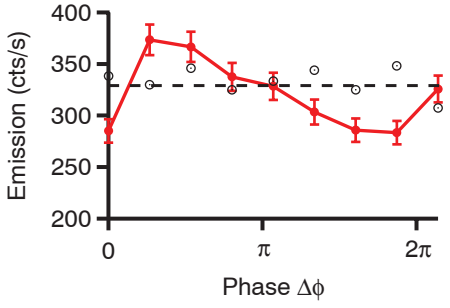

Fig. 3. Coherent phase control of the population transfer to the excited states of a single LH2 ring. Fluorescence signal of a single LH2 complex as a function of Δϕ at Δt = 150 fs (red). The emission features a 15% enhancement (reduction) compared with the reference signal (black symbols), that is, the emission upon excitation with a single transform-limited pulse covering the entire 120 nm spectral band width. Error bars, ±1 SD based on a total number of $N = 10^3$ photons.

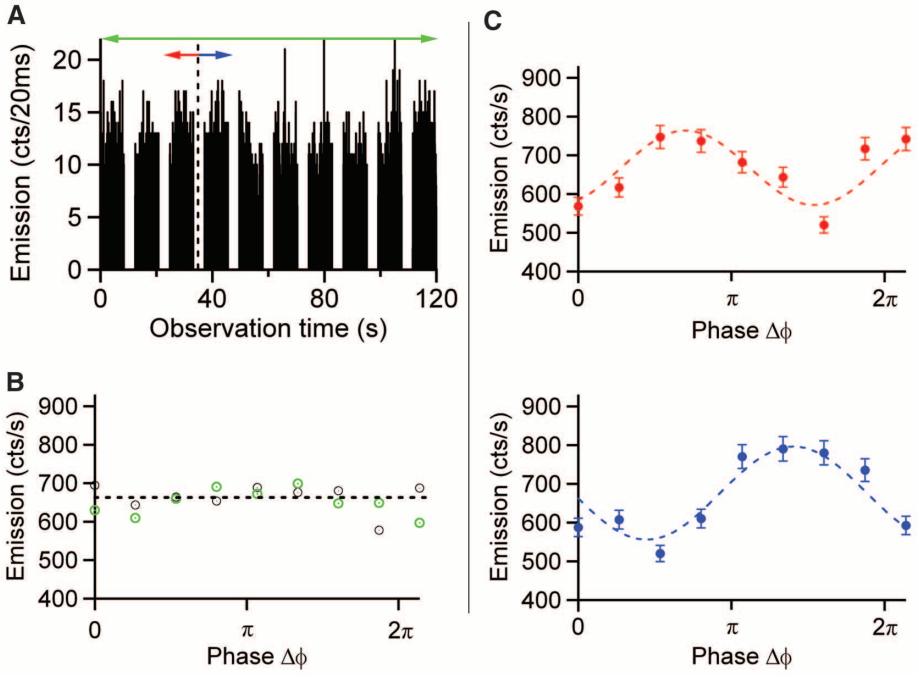

Fig. 4. Time-varying coherent energy transfer pathways. (**A**) Raw data from a single LH2 complex as a function of observation time: Each block represents a phase scan from 0 to 2π at Δt = 100 fs, interleaved with reference measurements using a single Fourier-limited pulse. (**B**) Reference signal (black symbols) and LH2 emission as a function of Δϕ temporally averaged over all 10 raw data blocks (green symbols). The dashed line is a guide to the eye representing the average signal. (**C**) Phase dependence of the LH2 emission averaged over the blocks left (red symbols, top) and right (blue symbols, bottom) of the dashed line in (A), considering only blocks with a constant reference signal. The red and blue dashed lines are cosine fits to the corresponding data, revealing a phase jump of about π after about 35 s of observation time. This is attributed to a modified energy transfer pathway within this single complex. Error bars, ±1 SD based on a total number of $N = 2 \times 10^3$ (top) and 1.5×10^3 (bottom) photons.

ments and thus possible pathways exist per ring, this is likely to be the optimal pathway for the particular geometrical and electronic structure, that is, for the specific electronic couplings. Moreover, the phase jumps observed for some assemblies (Fig. 4 and fig. S5) indicate that long-lived coherences also may provide flexibility to adapt to modifications of the (local) electronic structure and to find efficient new energy-transfer pathways within a complex. In other words, long-lived coherences contribute to the necessary robustness against external perturbations and disorder that are ubiquitous in biological systems at physiological temperatures. In this respect, the biological function of these complexes, light absorption and energy funneling toward the reaction center, is optimized for each individual aggregate, and long-lived quantum coherences herein play an important role.

References and Notes

1. R. J. Cogdell, A. Gall, J. Köhler, *Q. Rev. Biophys.* **39**, 227 (2006).
2. R. van Grondelle, V. I. Novoderezhkin, *Phys. Chem. Chem. Phys.* **8**, 793 (2006).
3. H.-M. Wu *et al.*, *J. Phys. Chem.* **100**, 12022 (1996).
4. J. L. Herek, W. Wohlleben, R. J. Cogdell, D. Zeidler, M. Motzkus, *Nature* **417**, 533 (2002).
5. J. L. Herek *et al.*, *Biophys. J.* **78**, 2590 (2000).
6. D. Kosumi *et al.*, *Angew. Chem. Int. Ed.* **50**, 1097 (2011).
7. G. D. Scholes, *Annu. Rev. Phys. Chem.* **54**, 57 (2003).
8. D. Beljonne, C. Curutchet, G. D. Scholes, R. J. Silbey, *J. Phys. Chem. B* **113**, 6583 (2009).
9. G. D. Scholes, *J. Phys. Chem. Lett.* **1**, 2 (2010).
10. M. A. Bopp, A. Sytnik, T. D. Howard, R. J. Cogdell, R. M. Hochstrasser, *Proc. Natl. Acad. Sci. U.S.A.* **96**, 11271 (1999).
11. A. M. van Oijen, M. Ketelaars, J. Köhler, T. J. Aartsma, J. Schmidt, *Science* **285**, 400 (1999).
12. D. Rutkauskas *et al.*, *Biophys. J.* **90**, 2475 (2006).
13. D. Brinks *et al.*, *Nature* **465**, 905 (2010).
14. R. Hildner, D. Brinks, N. F. van Hulst, *Nat. Phys.* **7**, 172 (2011).
15. C. Curutchet *et al.*, *J. Am. Chem. Soc.* **133**, 3078 (2011).
16. H. W. Kim, A. Kelly, J. W. Park, Y. M. Rhee, *J. Am. Chem. Soc.* **134**, 11640 (2012).
17. A. W. Chin *et al.*, *Nat. Phys.* **9**, 113 (2013).
18. S. Shim, P. Rebentrost, S. Valleau, A. Aspuru-Guzik, *Biophys. J.* **102**, 649 (2012).
19. S. Hoyer, A. Ishizaki, K. B. Whaley, *Phys. Rev. E* **86**, 041911 (2012).
20. K. A. Fransted, J. R. Caram, D. Hayes, G. S. Engel, *J. Chem. Phys.* **137**, 125101 (2012).
21. E. Harel, G. S. Engel, *Proc. Natl. Acad. Sci. U.S.A.* **109**, 706 (2012).
22. G. Panitchayangkoon *et al.*, *Proc. Natl. Acad. Sci. U.S.A.* **107**, 12766 (2010).
23. D. Zigmantas *et al.*, *Proc. Natl. Acad. Sci. U.S.A.* **103**, 12672 (2006).
24. T. Brixner *et al.*, *Nature* **434**, 625 (2005).
25. H. Lee, Y.-C. Cheng, G. R. Fleming, *Science* **316**, 1462 (2007).
26. V. I. Prokhorenko *et al.*, *Science* **313**, 1257 (2006).
27. G. Katz, M. A. Ratner, R. Kosloff, *New J. Phys.* **12**, 015003 (2010).
28. E. Collini *et al.*, *Nature* **463**, 644 (2010).
29. P. Rebentrost, M. Mohseni, I. Kassal, S. Lloyd, A. Aspuru-Guzik, *New J. Phys.* **11**, 033003 (2009).
30. M. B. Plenio, S. F. Huelga, *New J. Phys.* **10**, 113019 (2008).
31. M. Mohseni, P. Rebentrost, S. Lloyd, A. Aspuru-Guzik, *J. Chem. Phys.* **129**, 174106 (2008).

Acknowledgments: We thank F. D. Stefani, F. Kulzer, and T. H. Taminiau for discussions and assistance with the experimental setup. Funding by Ministerio de Ciencia e Innovación (CSD2007-046-NanoLight.es, MAT2006-08184, and FIS2009-08203), the European Union (European Research Council advanced grant no. 247330, FP6 Bio-Light-Touch), Fundació CELLEX (Barcelona) and the Biotechnology and Biological Sciences Research Council (Glasgow) is gratefully acknowledged. D.B. acknowledges support by a Rubicon grant of the Netherlands Organization for Scientific Research (NWO), and R.H. by the German Research Foundation (DFG, GRK 1640).

Supplementary Materials

www.sciencemag.org/cgi/content/full/340/6139/1448/DC1
Materials and Methods
Supplementary Text
Figs. S1 to S6
Table S1
References (*32*–*52*)

29 January 2013; accepted 13 May 2013
10.1126/science.1235820

Structure of Parkin Reveals Mechanisms for Ubiquitin Ligase Activation

Jean-François Trempe,[1]* Véronique Sauvé,[2]* Karl Grenier,[1] Marjan Seirafi,[2] Matthew Y. Tang,[1] Marie Ménade,[2] Sameer Al-Abdul-Wahid,[2] Jonathan Krett,[1] Kathy Wong,[2] Guennadi Kozlov,[2] Bhushan Nagar,[2] Edward A. Fon,[1]† Kalle Gehring[2]†

Mutations in the *PARK2 (parkin)* gene are responsible for an autosomal recessive form of Parkinson's disease. The parkin protein is a RING-in-between-RING E3 ubiquitin ligase that exhibits low basal activity. We describe the crystal structure of full-length rat parkin. The structure shows parkin in an autoinhibited state and provides insight into how it is activated. RING0 occludes the ubiquitin acceptor site Cys^{431} in RING2, whereas a repressor element of parkin binds RING1 and blocks its E2-binding site. Mutations that disrupted these inhibitory interactions activated parkin both in vitro and in cells. Parkin is neuroprotective, and these findings may provide a structural and mechanistic framework for enhancing parkin activity.

Parkinson's disease (PD) is a common neurodegenerative disease characterized by severe motor and nonmotor symptoms. More than 120 mutations in *PARK2* (*parkin*) have been shown to cause autosomal recessive PD, with point mutations found in every domain of the protein (*1*–*3*). The parkin protein is a RING-in-between-RING (RBR) E3 ubiquitin ligase (*4*) that exhibits low basal activity in vitro (*5*). Parkin has been implicated in a range of biological processes, including autophagy of damaged mitochondria (mitophagy), cell survival pathways, and vesicle trafficking (*6*, *7*). The activity of the PD-associated mitochondrial kinase PINK1 is required for parkin activation in mitophagy (*8*–*12*). Parkin consists of a ubiquitin-like (Ubl) domain and a 60–amino acid linker followed by RING0, a zinc finger unique to parkin (*13*), and three additional zinc finger domains characteristic of the RBR family (Fig. 1A). RBR ligases such as parkin, HOIL-1L interacting protein (HOIP), and Ariadne/HHARI use a RING-HECT hybrid mechanism (*14*–*16*) whereby ubiquitin forms a thioester intermediate with a cysteine side chain in RING2 before being transferred to the primary amino group of a substrate to form an isopeptide bond. How RBR ligases accomplish these two reactions is unknown.

We determined the crystal structure of rat parkin, obtaining a low-resolution structure of the full-length protein and a 2.8 Å resolution structure of a C-terminal fragment (amino acids 141 to 465) (Fig. 1B, figs. S1 and S2, and table S1). Collectively, the structures show that parkin forms a rigid core of the RING0, RING1, and RING2 domains stabilized by several key hydrophobic interactions (Fig. 1C). This core functions as a scaffold for interactions with the remaining domains of parkin. The in-between-RING (IBR) domain is attached through a flexible linker; its position varies by up to 13 Å between different chains in the structure of the C-terminal fragment (fig. S2B). The N-terminal Ubl domain is bound to RING1 through the hydrophobic surface centered around Ile^{44}, consistent with the reported interaction between the Ubl and the C terminus (*5*). This surface of the Ubl also binds ubiquitin-interacting motifs (*17*–*19*) (UIMs) and SH3 domains (*20*), implying that the Ubl must dissociate from RING1 in order to bind these partners. The long linker following the Ubl is not visible in the crystal structure, but a fragment of the second linker between the IBR and RING2 domains is visible. This fragment contains an α helix bound to RING1, called REP (repressor element of parkin).

[1]McGill Parkinson Program, Department of Neurology and Neurosurgery, Montreal Neurological Institute, McGill University, Montréal, Québec H3A 2B4, Canada. [2]Groupe de Recherche Axé sur la Structure des Protéines and Department of Biochemistry, McGill University, Montréal, Québec H3G 1Y6, Canada.

*These authors contributed equally to this work.
†Corresponding author. E-mail: kalle.gehring@mcgill.ca (K.G.); ted.fon@mcgill.ca (E.A.F.)